Role of electric and magnetic dipole strength functions in the ^{114}Cd(γ,γ') and ^{113}Cd(n,γ) reactions

R. Massarczyk,[1,2,*] G. Schramm,[3,2] T. Belgya,[4] R. Schwengner,[1] R. Beyer,[1] D. Bemmerer,[1] Z. Elekes,[1] E. Grosse,[1,2] R. Hannaske,[1,2] A. R. Junghans,[1] Z. Kis,[4] T. Kögler,[1,2] C. Lorenz,[1] K. Schmidt,[1,2] L. Szentmiklósi,[4] A. Wagner,[1] and J. L. Weil[4]

[1]*Helmholtz-Zentrum Dresden-Rossendorf, Institute of Radiation Physics, D-01328 Dresden, Germany*

[2]*Technische Universität Dresden, Institute of Nuclear and Particle Physics, D-01062 Dresden, Germany*

[3]*Helmholtz-Zentrum Dresden-Rossendorf, Institute of Radiopharmacy, D-01328 Dresden, Germany*

[4]*Centre for Energy Research, Hungarian Academy of Sciences H-1525 Budapest 114, Post Office Box 49, Hungary*

(Received 4 May 2015; revised manuscript received 29 August 2015; published 5 January 2016)

The distribution of the electromagnetic dipole strength below the neutron separation energy and its influence on the photon distribution after neutron capture were investigated in two experiments for the compound nucleus ^{114}Cd. By measuring the photoabsorption cross section at the bremsstrahlung facility γELBE at Helmholtz-Zentrum Dresden-Rossendorf it was possible to deduce the distribution of dipole strength below the neutron separation energy. The de-excitation spectrum after cold-neutron capture in ^{113}Cd was measured at the Budapest Neutron Center. In a combined analysis, the experimentally deduced spectra after photon scattering on ^{114}Cd and the neutron capture in ^{113}Cd were analyzed in terms of electric and magnetic strength functions and nuclear level density with the help of the statistical code γDEX.

DOI: 10.1103/PhysRevC.93.014301

I. INTRODUCTION

Future nuclear facilities like the Multi-purpose hYbrid research reactor for high-tech applications project [1] aim for the transmutation of nuclear waste with long half-lives. These facilities are planned and simulated in advance to guarantee an efficient transmutation process. Detailed data, like cross sections for fission, neutron scattering and capture, or photonuclear reactions, are needed for many isotopes. These quantities can be measured for stable isotopes but for many short-lived isotopes participating in the reaction chain it is impossible get experimental information. Theoretical models and global predictions replace the nonexisting experimental information. However, theory and parametrization have to show their validity in experiments on stable nuclei.

Two of these quantities which are of special interest are the photon strength function and the nuclear level density, which directly enter in statistical model calculations, e.g., the description of the photon spectrum after neutron capture.

In two previous experiments [2,3] we used the general assumption that the de-excitation of nuclear states should be independent by the excitation method. We were able to show that there is no deviation from this principle for states around the neutron separation energy. The average radiative decay in a compound nucleus of a state at this excitation energy can be described by statistical quantities, namely nuclear level density and photon strength function (PSF). In a detailed view the decay pattern of single states are affected by nuclear structure but these two quantities can be used to describe quantities like energy distribution or multiplicity of γ rays after neutron capture.

The two nuclei ^{78}Se and ^{196}Pt have been chosen first as representatives for different mass regions. Both nuclei have been investigated in combined experiments via neutron capture at the research reactor in Budapest and via photon scattering at the electron accelerator Electron Linac with high Brilliance and low Emmitance (ELBE) in Dresden. As shown in Fig. 1, nuclear states with the same spin and parity are excited with two different excitation mechanisms. In the first experiment, a single state is excited by the capture of a cold neutron in the neighboring isotope. This state decays via the emission of one or more photons. In the second type of experiment, states with the spin 1 and mainly negative parity are excited up to the neutron separation threshold by the irradiation of the target nucleus with bremsstrahlung. The decay spectra are recorded in both experiments, respectively. These spectra contain transitions to the ground state and information from photons which are produced in the de-excitation of the excited nucleus through a cascade of intermediate states. Level density and strength function have a major impact on the transition widths and influence the energy distribution the photons.

Nevertheless, the nuclear level density and strength function are often handled and extracted from experiments independently. For the nucleus ^{114}Cd information on excited states at lower excitation energies is available [4], especially from earlier neutron-capture experiments with a thermal neutron spectrum [5,6]. In these experiments properties of the low-energy states such as branching ratio, spin, and parity were determined. The prominent transitions occur also in the de-excitation spectra of our experiments. The increasing level density prevents a full spectroscopic analysis of the spectrum due to the finite detector resolution. At an excitation energy of about 5 MeV the average level spacing falls below the detector resolution of high-purity germanium detectors. Single transitions between excited states cannot be resolved anymore. The approach of analyzing the quasicontinuum of states as done in previous experiments [2,3,7–9] can be used to derive information about the nuclear level density and strength function in the continuum of unresolved states in the final nucleus.

The complete photon strength consists of different strength functions with different character, magnetic or electric, in

*Present address: Physics Division, Los Alamos National Laboratory, Los Alamos, New Mexico 87545, USA.

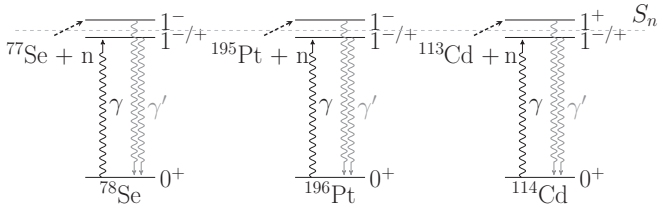

FIG. 1. Overview of the spin and parity of the states, which are mainly excited in neutron capture and nuclear resonance fluorescence experiments.

different multipole orders. The dominating strength is the electric dipole strength. Its distribution shows a characteristic resonance around 15 to 20 MeV, the giant dipole resonance (GDR). Experimental information about this resonance structure is often used to fit the distribution of dipole strength as a function of excitation energy with one or more Lorentzian functions [10,11]. These functions can be extrapolated towards lower energies and used to describe the tail of the GDR where often no information is available. Strength in this energy region plays a major role in the radiative de-excitation of states. For the isotope ^{114}Cd, no detailed information for reaction with photons is available, but for natural cadmium the (γ,n) cross section has been measured and can be used for comparison [12]. The natural abundance of ^{114}Cd in $^{\text{nat}}$Cd is 28.73%.

In contrast to the two previous experiments on ^{78}Se and ^{196}Pt, the dominantly excited states in ^{114}Cd after neutron capture have spin and parity of $J^\pi = 0^+$ and 1^+. In combination with the ground-state property $J^\pi = 0^+$ the direct ground-state transition has to be a magnetic dipole transition, cf. Fig. 1, since the parity is conserved. Of, course transitions with higher multipole order transitions like $E2$ are possible but usually lower orders are favored. This feature is the motivation to have a closer look at the influence of the magnetic dipole distribution on the description of the experimental results.

The combined analysis of data from cold-neutron capture and photon scattering allows a better investigation of the interaction of the two quantities, strength function and level density. As in previous papers, the statistical code γDEX [2] is used to correct and describe spectra in both experiments. In combination with detector simulations using GEANT4 [13] we were able to correct for the influence of detector response, detector efficiency, and atomic background.

This paper will present only briefly the experimental facilities and methods because the experimental method is very close to that used in the previous twin experiments. The results of the γDEX simulations and a discussion of the impact of different models will be given.

II. PHOTON SCATTERING AT ELBE

The photoabsorption cross section was determined from the spectra measured in a photon scattering experiment at the bremsstrahlung facility γELBE [14]. The electrons of the ELBE accelerator of the Helmholtz-Zentrum Dresden-Rossendorf produce thin-target bremsstrahlung when impinging onto a 12-μm-thin niobium foil. This method provides

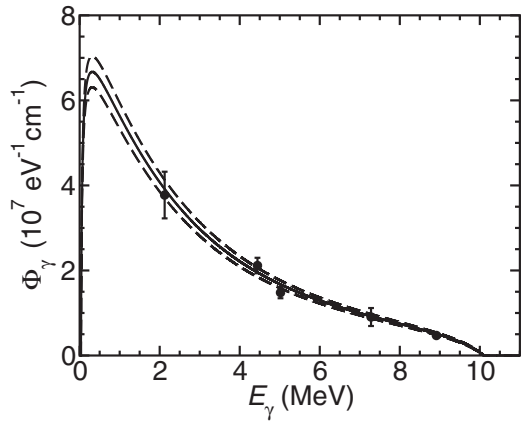

FIG. 2. Spectral bremsstrahlung fluence at the target deduced from transitions in ^{11}B (black circles). The solid black line shows the calculated fluence distribution using the Schiff distribution [15], and the dashed lines show the uncertainty of the photon fluence.

photons with a broad energy distribution. The energy of the electrons was chosen to be $p_{e^-}c = 10.5$ MeV and ensures photons with a maximum energy $E_\gamma > S_n$. The neutron separation threshold of ^{114}Cd is $S_n = 9.043$ MeV. The photons pass through a 10-cm-thick aluminum beam hardener, which increases the ratio of high-energy to low-energy photons. Subsequently, the beam is shaped by a 2.6-m-long aluminum-made collimator which is set in the wall to the experimental cave. At the target position the photon fluence can be determined with the help of the known cross sections of individual states in ^{11}B [16–18], cf. Fig. 2. For this purpose, 200 mg of enriched boron powder were placed in front of the target. The ^{114}Cd target itself had a weight of 2.001 g and had been enriched to 99.37 % isotopic abundance.

The scattered photons were detected with four high-purity germanium detectors (HPGe) placed in two pairs. One pair of detectors was situated at 90° whereas the other pair was placed at 127° with respect to the incoming photon beam. Each detector is surrounded by a bismuth-germanate scintillation detector acting as a veto detector against cosmic ray interactions and as γ escape suppression shield.

The integrated photoabsorption cross section $I_{\text{abs}} \approx \overline{\sigma_\gamma}\,\Delta E$ within an energy bin ΔE can be calculated in relation to the photon fluence:

$$I_{\text{abs}} = \frac{Y_{\text{abs}}(E,\Delta E)}{W(E_\gamma,\theta)\Phi_\gamma(E_x)N_N\, b_0(E_x)}. \qquad (1)$$

In this equation the angular correlation factor $W(E_\gamma,\theta)$ is used to weight the yield from both detector pairs. The orientation of the detectors relative to a beam is optimized for the detection of dipole radiation. It has be shown in different previous experiments [9,19] that detected discrete lines are of a dipole nature. The final cross section is a combination of the results from both pairs of detectors. For each pair the cross section is determined and the combined average presented in Fig. 3. They agree within the error bars. The photon fluence $\Phi_\gamma(E_x)$, the number of target atoms N_N, and the average ground-state branching ratio $b_0(E_x)$ are needed. The detector

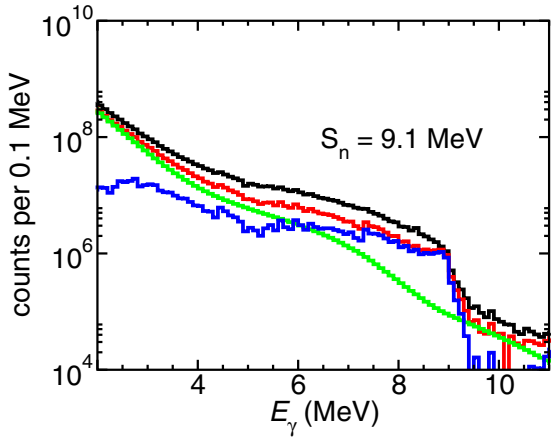

FIG. 3. Measured spectrum in the different analysis steps for the detector pair under 127°. The spectrum corrected for natural background (black), the spectrum unfolded for detector response (red [gray]), the simulated atomic background (green [light gray]), and the subtracted spectrum (blue [dark gray]).

efficiency was simulated with GEANT4 over the full energy range for each detector. The comparison with the spectra from radioactive standard sources was performed and a good agreement between simulation and experimental data points was found [19]. The photon fluence normalized to the photon absorption in boron is shown in Fig. 2 with the calibration values of transitions from the ^{11}B monitor. The measured yield $Y_{\rm meas}(E,\Delta E)$ in an energy interval ΔE at photon energy E has to be corrected for several interfering processes in order to get the desired absorption yield $Y_{\rm abs}$:

$$Y_{\rm abs}(E,\Delta E) = \frac{Y_{\rm meas}(E,\Delta E) - Y_{\rm back}(E,\Delta E) - Y_{\rm resp}(E,Y(E'),\Delta E)}{\epsilon(E,\theta)} - Y_{\rm atomic}(E,\Delta E) - Y_{\rm inelas}(E,Y(E''),\Delta E). \quad (2)$$

Thus, the following steps were performed to determine the yield from the measured photon scattering data:

(1) Subtraction of ambient background $Y_{\rm back}(E,\Delta E)$.
(2) Unfolding of the measured spectrum for detector response $Y_{\rm resp}(E,E',\Delta E)$. The yield which is seen at an energy E is overestimated. γ rays with higher energies $E' > E$ can deposit less than their full energy inside the detector. The detector response function is deduced from simulations with GEANT4 in which monoenergetic γ rays were emitted from the target position isotropically. The energy of the photons sent out was decreased in 10-keV steps. The simulated spectra were normalized to the photo peak in each bin of the measured spectrum and subtracted, starting with the highest energy. The spectrum strip method [20] removes the events which have not deposited their full energy within the detector. The uncertainty caused by the deconvolution is small for each bin, but the uncertainties add up while going downward in energy from bin to bin. For lower energies the errors are in the range of 25% [2,3,19]. After these two subtractions the spectrum is corrected for the full-energy detection efficiency.
(3) Subtraction of the non-nuclear (atomic) background $Y_{\rm atomic}(E,\Delta E)$ which is also simulated with GEANT4.
(4) Subtraction of inelastic transitions $Y_{\rm inelas}(E,Y(E''),\Delta E)$. The yield at an energy E can contain also γ rays from inelastic scattering from higher energy states with $E'' > E$. Therefore, the yield at lower energies depends on the yield at higher energies.
(5) Finally, the spectrum contains only information from elastically scattered photons registered with their full energy in the detector. In order to get the full photon absorption cross section, the ground-state branching ratio b_0, which describes the ratio of elastic scattering to total scattering, is calculated for each excitation energy. The yield is corrected for this branching and takes into account the elastic enhancement introduced in Ref. [2].

The different steps in analysis and their impact on the spectrum can be seen in Fig. 3. It shows the response-corrected experimental spectrum and the yield due to non-nuclear scattering in the target. The latter one was calculated with a GEANT4 simulation, multiplied with the detector efficiency and adjusted to the experimentally deduced photon flux. The subtracted spectrum is shown and it can be seen that for transition energies above 7 MeV the spectrum is scarcely affected by the atomic background.

The broad continuum of unresolved transitions is used as an input for the γDEX simulation in order to estimate the influence of inelastically scattered events. The average branching ratio in an energy bin is also a result of these simulations. To run this simulations, strength functions and nuclear level density function are needed.

As a first input for the electric dipole strength, the triple Lorentzian model (TLO) [11] is used. The quadrupole deformation parameter is $\beta_2 = 0.19$ [21]. With the systematics of Ref. [22] a triaxiality parameter of $\gamma \approx 22°$ can be estimated. After a first iteration using the TLO approach as description of the electric dipole strength, the output is used to calculate a new strength function which works as input for the next iteration step. Assuming that photo absorption is dominated by dipole excitations, the summed dipole strength function $f_1 = f_{E1} + f_{M1}$ can be calculated using the relation derived in Ref. [23]:

$$\langle \sigma_{\gamma,\rm abs} \rangle = 3(\pi\hbar c)^2 E_\gamma f_1(E_\gamma). \quad (3)$$

The new generated dipole strength is fitted with a smooth function [2]. This function contains the following:

(1) The tail of the GDR. The TLO description is multiplied with a free energy-independent parameter. By doing so the shape is not changed, just the absolute height. The data points from Ref. [12] are included in this fit so a smooth transition to the data points of the (γ,n) experiments is achieved.
(2) An extra Lorentzian function to the electric dipole strength which takes into account the extra strength around 4 MeV.

The magnetic dipole part. This is adjusted to the $E1$ strength for the RIPL3 description. The three-Gaussian description is not changed.

This function guarantees a smooth description of the dipole strength below $E_\gamma < 4$ MeV where the experimental uncertainties are too big to give a reasonable description. The iterative procedure is performed until the output strength is in accordance with the input for all data points above 4 MeV within uncertainties.

This iterative method is performed for all calculations shown in this work. Also the branching ratio b_0 is estimated with this calculation and newly determined in each iteration step.

For the magnetic dipole strength function two models are discussed in this work:

(1) RIPL3 M1 model [10]. In this model the $M1$ strength is described as one Lorentzian-shaped resonance. The absolute height of the resonance is adjusted to the electric dipole strength at $E_x = 7$ MeV. The position of the resonance is given as $E_r = 41\ A^{-1/3}$ MeV. The width of the resonance is independent from the mass of the nucleus and fixed to $\Gamma_r = 4$ MeV.

(2) Triple Gaussian model [2]. This model describes the $M1$ strength distribution with three Gaussian shaped peaks. One describes the scissors mode, one the isovector mode, and one the isoscalar spin-flip mode. Integral and resonance position are dependent on the mass of the nucleus and the nuclear deformation. The description of the three components is given in Ref. [2]. The deformation parameters are the same as used in the TLO model.

The two models differ in the integrated strength as well as in the shape of the distribution. For the $E2$ strength function the RIPL3 recommendation is used. The parametrization of this depends only on the nucleon number A and Z.

The nuclear level density is calculated with the model described in Ref. [24]. The level density is factorized into an energy-dependent part, a spin-dependent part, and a parity distribution. For the parity distribution the model given in Ref. [25] was used since in Ref. [24] no detailed parity model is given. It predicts a smooth transition to an equal distribution of positive and negative parities at higher energies with a smooth transition to a dominant regime of positive parities at lower excitation energies. The spin distribution is that of Ref. [24] which uses an A- and Z-dependent calculation for the spin cutoff parameter. The predicted staggering of even spins in even-even nuclei is used but smoothed out so it disappears at higher excitation energies. This smoothing takes into account the findings of theoretical calculations given in Ref. [26]. For the energy dependence, the constant-temperature model is used, which has two parameters. The temperature parameter T describes the slope of the nuclear level density versus the excitation energy. The back-shift energy E_0 is used to adjust the level density at the neutron separation threshold to the measured level spacing $D_0 = 24.8$ eV [27]. Within the statistical code, information on the first 26 exited states

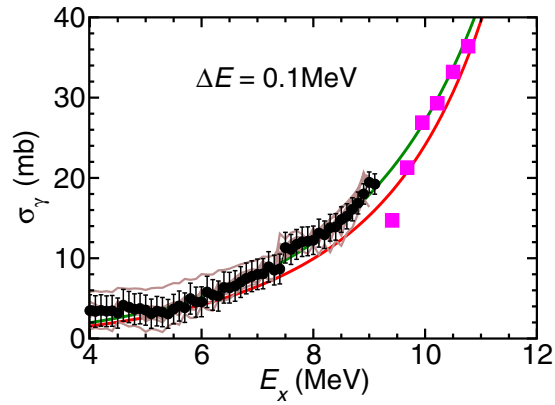

FIG. 4. Photo-absorption cross section deduced at ELBE (black points) in combination with the prediction of the TLO model (red [gray] line) and the RIPL3 prediction with two Lorentzian functions (green [light gray] line). In addition, the outputs for the electric dipole strength function during the iterations of the analysis (brown [dark gray] lines) and the first few data points (pink [very light gray]) of the (γ,n) experiment [12] are shown.

($E_x{}^{26} = 2.46$ MeV) is explicitly included, with their spins and parities as well as their branching ratios [4].

In combination with the information of the neutron capture experiment the temperature is varied to optimize the fit to the measured photon spectrum after neutron capture, described in next section. The literature value of the temperature is $T = 670(20)$ keV [24], whereas the best agreement of our simulations and experimental data in this work was found for a temperature value of $T = 640(15)$ keV; cf. the following discussion about neutron capture results. The final cross section result using this value is shown in Fig. 4. The iterative development of the distribution is shown as well as some data points from a $^{\text{nat}}$Cd (γ,n) experiment [12].

As one can see in Fig. 4 the determined cross section agrees well with the general trend of the predictions by RIPL3 and the TLO models. A smooth connection to the data measured for $^{\text{nat}}$Cd is also found. A significant excess of the dipole strength, for which often the term *pygmy resonance* [28] is used, can not be seen. In previous experiments using the same method we have found a significant excess of the tail of the giant dipole resonance. A strong evidence for a pygmy resonance can for example be found in ^{78}Se [2].

The neighboring even-even isotope ^{112}Cd has been studied at the Oslo Cyclotron Laboratory using the $(^3\text{He}, ^3\text{He}')$ reaction [29]. A dipole strength function was deduced and can be compared by the one calculated from the results of this work. Between neighboring isotopes we expect only a small difference in the strength functions. Therefore, the absorption cross section was transformed to a strength function by using Eq. (3) under the assumption of a dominating dipole nature. As one can see in Fig. 5 the results agree above 7 MeV. Towards lower energies a discrepancy is found. In both experiments, photon and ^{3}He scattering, no explicit distinction between magnetic and electric dipole strength can be done, so the complete dipole strength has to be compared. Differences in the results might be explained by different

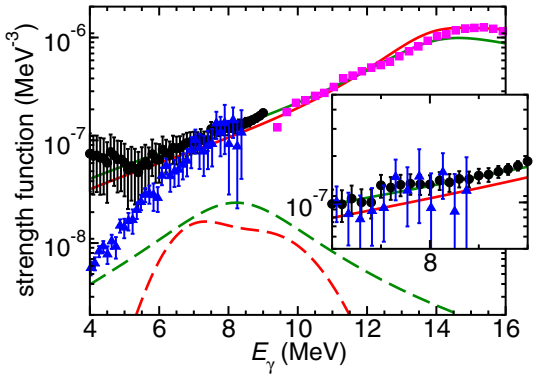

FIG. 5. Comparison of the strength functions deduced from the present measurement and different models. The symbols are the same as in Fig. 4. In addition the strength function of ^{112}Cd deduced from ^{3}He scattering [29] (blue [dark gray] triangles) is shown. The magnetic dipole strength functions from RIPL3 (green [light gray] dashed line) and for the three Gaussian models (red [gray] dashed lines) are also plotted. The inset shows the region close to the neutron separation energy in detail.

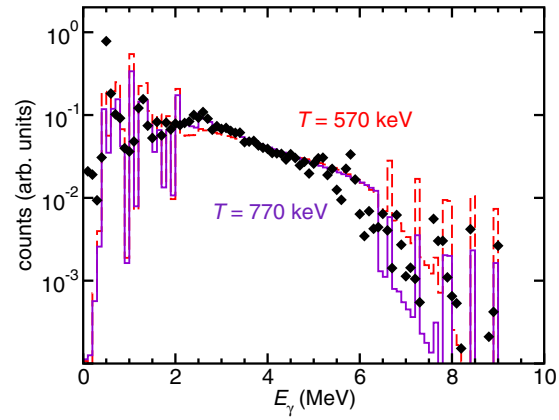

FIG. 6. Comparison of different simulation calculations with the measured and response corrected γ-ray spectrum (black diamonds) after neutron capture. The temperature parameter used in γDEX was varied from 570 (dashed violet [dark gray]) to 770 keV (solid red [gray]). Both simulations were performed with the TLO model for electric dipole strength and with the triple Gaussian model for magnetic dipole strength and should show for one pair of strength function how the nuclear level density can change the shape of the de-excitation spectrum. The uncertainties for the experimental data are 10% at higher energies and are increasing towards 25% at 1 MeV excitation energy.

excitation mechanisms. The isoscalar and isovector parts of the strength functions are excited by ^{3}He while it is expected that photons only excite the isovector part. Another difference can be found in the spin distribution of the excited states. While photons excite spins close to the ground-state spins, the reaction mechanism in ^{3}He scattering allows the excitation of higher spin ranges.

III. NEUTRON CAPTURE IN BUDAPEST

As in the other twin experiments, the neutron-capture experiment took place at the 10-MW research reactor in Budapest. At the prompt γ activation analysis (PGAA) setup [30] it is possible to measure γ rays after cold-neutron capture. A bismuth germanate-guarded 27% HPGe detector system was used for the detection of photons. The detector and the target chamber were covered with ^{6}Li-filled plastic sheets. These foils reduce the amount of neutrons scattered from the target in order to avoid nontarget neutron-capture reactions. In addition, the influence of background was investigated by an empty-target measurement. The target was an enriched (90.2%) high-purity cadmium metal with a total mass of 0.1 g. The beam size was reduced to 1 mm^2 to avoid the extraordinarily high count rate arising from the very high neutron-capture cross section.

The measured photon spectrum was corrected for natural and beam-induced background. After that, the spectrum was unfolded with the detector response function and detection efficiency [2,3,31].

In Fig. 6 the influence of the level density on the simulated γ-ray spectrum after neutron capture is shown. Above 6.5 MeV the spectrum is characterized by transitions to low-lying states, which are implemented in the γDEX code. Below 2 MeV, again the de-excitation of these low-lying states dominates the spectrum except for a few low-energy transitions between higher-lying states. Due to the deconvolution algorithm this part of the corrected data has the largest uncertainty. It is influenced by the response functions from γ rays with higher energies. Between these two regions a broad continuum can be seen, in which events caused by transitions between intermediate states and other intermediate states, the ground state, or the initial capture state can be found. In this quasicontinuum of unresolved transitions the statistical models can be applied.

A large number of states contribute to this region and under the assumption of the Axel-Brink hypothesis [32,33] the strength function depends only on the transition energy but not on the excitation energy of the states. The simulations discussed in this section are adjusted in its number to the counts in this broad continuum with an energy-independent weighting factor. This factor is chosen in such a way that the number of events between 2 and 7 MeV in simulation and experiment corrected for detector response and efficiency best agree with each other.

In the different simulations shown in Fig. 6, the temperature value was varied in a range of 570 to 770 keV. As discussed before, the back shift energy is adjusted in order to reflect the measured density of states at the neutron separation threshold. For each temperature value the electric dipole strength function in photon scattering experiment was determined again and used in γDEX as input. As one can see, the slope of the continuum of unresolved states between 2 and 7 MeV is influenced on a small scale by the temperature parameter. Of course, the ratio of the intensities of discrete transitions to the intensity in the continuum is changing. Nuclear temperature values around the literature value of $T = 670$ keV result in a good description of the continuum of unresolved transitions.

In Fig. 7 the second important ingredient, strength function, is varied. For different strength-function combinations the

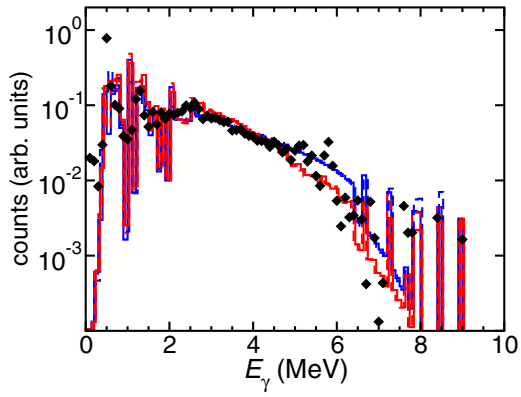

FIG. 7. Comparison of the measured and response-corrected γ-ray spectrum (black diamonds) after neutron capture with different simulation results. Various combinations of strength functions were used in each data set, while the temperature value was fixed to $T = 670$ keV. The red (gray) lines show that the TLO model was used as input in the simulation, and the blue (dark gray) ones stand for the usage of the $E1$ strength function determined at ELBE. The solid lines indicate the usage of the three-Gaussian model as $M1$ strength function whereas the dashed lines stand for the RIPL3 parametrization of the magnetic dipole strength.

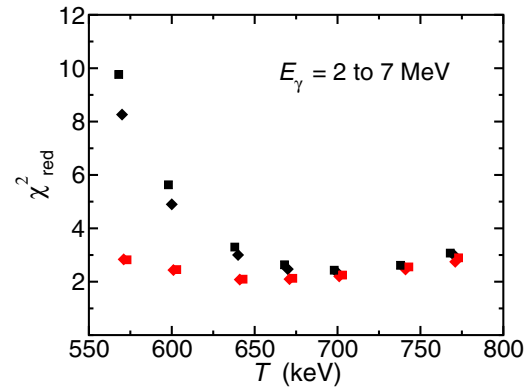

FIG. 8. Reduced χ^2 value for the comparison between the simulation outputs and the experimental spectrum for photon energies between 2 and 7 MeV. Different models are used as simulation input: the triple-Lorentzian model (black) and the iteratively experimental deduced electric strength function (red [gray]) for the electric dipole strength and the RIPL3 parametrization (open diamonds) and the Gaussian model (filled squares) for the magnetic strength. The experimental deduced dipole strength is retrieved separately for each temperature value.

spectrum is calculated. For a temperature value of $T = 670$ keV the photon spectra after neutron capture for different combinations of electric and magnetic dipole strength functions are shown. As one can see, different electric dipole strength functions have a significant effect on the slope of the continuum while the magnetic dipole strength has only little effect. This means the electric dipole distribution influences the de-excitation cascade more than the magnetic dipole strength.

As one can see in both figures, the slope of the continuum is influenced by both level densities and photon strength function. Hereby, the level density seems to play a minor role while a change in the strength function can cause larger changes. In order to investigate both parameters, strength function and level density, simultaneously the data sets from Dresden and Budapest have been analyzed in a combined way. For various temperature values different strength function combinations from Fig. 7 are used as input. For γ rays with energies between 2 and 7 MeV the different simulation outputs are compared with the experimental spectrum. In Fig. 8 the χ^2_{red} values, which describe the goodness of agreement between each calculation and experimental neutron capture spectrum, can be seen. The overall agreement is improved when using the experimentally deduced strength function. The different magnetic strength functions have only a small impact on the results, which means that the electric dipole strength dominates the de-excitation process. The spin-parity combination of the capture state is one reason for this behavior. At a first glance for the direct decay to the ground state a magnetic dipole transition is the only possibility and therefore the magnetic character of the radiation seems to be more important in this decay as in the previous measured nuclei. But for transitions from the capture state into intermediate energy states the electric dipole strength is stronger than the magnetic one. These electric dipole transitions cause a change into states with negative parity. Now, such a state has to decay again via an electric dipole transition in order to reach one of the low-lying states with positive parity. In contrast to the previously studied nuclei (^{78}Se and ^{196}Pt) a cascade now has to consist of an even number of $E1$ transitions. In the two other examples a de-excitation of one electric dipole transition with a transition of another multipole character is possible. In ^{114}Cd one electric dipole transition causes automatically a second. This fact explains the strong influence of the electric dipole strength to the photon distribution in Fig. 7 and the significant improvement in Fig. 8 when using the determined experimental strength distribution.

The overall temperature dependence is weak, as stated before, especially when the dipole strength is calculated separately for each temperature. The reason for this behavior is that the strength function determined from photon scattering for each temperature value can still describe the de-excitation scheme after neutron capture quite well. This is very strong evidence that it is suitable to describe the de-excitation of nuclear states in this energy region with statistical quantities. Especially at the literature value of the temperature, one can see that a different strength function causes only a small change in the χ^2 value. Using different electric, TLO or experimental, or magnetic, RIPL or three-Gaussian, methods causes only minor differences in the description of the γ-ray spectrum after neutron capture. Going further away from the literature value, one can see that a change of the magnetic dipole strength also causes only small differences. When using a fixed strength function, one can see that a clear minimum is reached. As mentioned before, the best description is found for a temperature value of 640(15) keV. For this temperature value a γ-ray multiplicity of 3.8 ± 0.3 was found in the γDEX calculations. This value is in agreement with findings in previous neutron-capture experiments in which a value of 4.1 is

reported [34]. Detailed studies of the photon distribution show also that an average photon multiplicity of four is reached in the decay of an excited state in ^{114}Cd at $E \approx S_n$ [35]. This high multiplicity can be explained by the behavior discussed before.

The experimentally deduced photo-absorption cross section from ELBE was transformed into a strength function, assuming a dominating dipole character. Using the temperature value of $T = 640$ keV one can calculate a level density ϱ and in combination with the strength function f the total γ width $\Gamma_{\rm tot}$. The individual transition widths to all possible final states j for all primary γ-ray transitions from the capture state can be summed up [23]:

$$\Gamma_{\rm tot} = \sum_j \varrho(E_j)\left(E_{S_n} - E_j\right)^3 f\left(E_{S_n} - E_j\right). \qquad (4)$$

Here, j reaches over the whole energy range from 0 up to S_n. The total γ width determined for this work is $\Gamma_\gamma = 96(10)$ meV. This calculated value is compatible to the experimental value of the radiative width $\Gamma_\gamma = 113(1)$ meV [27] of the nearest s-wave resonance and also close to the average radiative width of the 10 lowest s-wave resonances [36], where $\Gamma_\gamma = 113.5(1)$ was found.

IV. CONCLUSIONS

The combined analysis of the data from two different experiments allowed us to study the effect of different electric and magnetic dipole strength functions in the decay of excited states in the same final nucleus. The information from photon scattering was used to determine the photo-absorption cross section in ^{114}Cd. The transformation from cross section into strength function allowed us to investigate the level densities in the nucleus ^{114}Cd. The γDEX code was used for this purpose in both analyses. By taking into account the quasicontinuum of unresolvable states and transitions, the full strength was taken into account and the photon spectrum after neutron capture can also be described reasonably well. The dipole strength function determined below the neutron separation energy follows a smooth trend of the tail of Lorentzian fits of the GDR. No evidence is seen for the pygmy resonance seen in our other similar studies. The s-wave neutron capture on a spin-$1/2^+$ target nucleus allowed, in principle, the investigation of the influence of the magnetic dipole strength. The magnetic strength function cannot be determined separately in the experimental method used in this work. Different models have been tested in the analysis and their influence on the experimental results is presented. Since the $E1$ strength fitted the data well and the $M1$ strength is almost an order of magnitude weaker than the dominant $E1$ strength, it was not possible to learn anything significant about the $M1$ strength. The constant-temperature model was used for the description of the nuclear level density. The number of possible states in the de-excitation cascade was varied by the temperature parameter. The value $T = 640(15)$ keV, which gives the best agreement, is slightly lower than the literature value.

ACKNOWLEDGMENTS

We thank the staffs of the ELBE accelerator and the Budapest Research Reactor for their cooperation during the experiments and A. Hartmann for the technical assistance. Also we thank A.C. Larsen for helpful discussions. Both experiments were supported in part by the EURATOM FP7 project ERINDA (FP7-269499), the Hungarian project OMFB 00184/2006 NAP VENEUS05, and the German BMBF project TRAKULA (02NUK013A).

[1] H. Abderrahim *et al.*, Nucl. Instr. Meth. A **463**, 487 (2001).
[2] G. Schramm, R. Massarczyk, A. R. Junghans, T. Belgya, R. Beyer, E. Birgersson, E. Grosse, M. Kempe, Z. Kis, K. Kosev, M. Krticka, A. Matic, K. D. Schilling, R. Schwengner, L. Szentmiklosi, A. Wagner, and J. L. Weil, Phys. Rev. C **85**, 014311 (2012).
[3] R. Massarczyk, G. Schramm, A. R. Junghans, R. Schwengner, M. Anders, T. Belgya, R. Beyer, E. Birgersson, A. Ferrari, E. Grosse, R. Hannaske, Z. Kis, T. Kogler, K. Kosev, M. Marta, L. Szentmiklosi, A. Wagner, and J. L. Weil, Phys. Rev. C **87**, 044306 (2013).
[4] J. Blachot, Nucl. Data Sheets **113**, 515 (2012).
[5] A. Mheemeed *et al.*, Nucl. Phys. A **412**, 113 (1984).
[6] F. Braumandl *et al.*, Nucl. Instrum. Methods **166**, 243 (1979).
[7] R. Massarczyk, R. Schwengner, F. Donau, S. Frauendorf, M. Anders, D. Bemmerer, R. Beyer, C. Bhatia, E. Birgersson, M. Butterling, Z. Elekes, A. Ferrari, M. E. Gooden, R. Hannaske, A. R. Junghans, M. Kempe, J. H. Kelley, T. Kogler, A. Matic, M. L. Menzel, S. Muller, T. P. Reinhardt, M. Roder, G. Rusev, K. D. Schilling, K. Schmidt, G. Schramm, A. P. Tonchev, W. Tornow, and A. Wagner, Phys. Rev. Lett. **112**, 072501 (2014).
[8] R. Schwengner, R. Massarczyk, G. Rusev, N. Tsoneva, D. Bemmerer, R. Beyer, R. Hannaske, A. R. Junghans, J. H. Kelley, E. Kwan, H. Lenske, M. Marta, R. Raut, K. D. Schilling, A. Tonchev, W. Tornow, and A. Wagner, Phys. Rev. C **87**, 024306 (2013).
[9] R. Massarczyk, R. Schwengner, L. A. Bernstein, M. Anders, D. Bemmerer, R. Beyer, Z. Elekes, R. Hannaske, A. R. Junghans, T. Kogler, M. Roder, K. Schmidt, A. Wagner, and L. Wagner, Phys. Rev. C **92**, 044309 (2015).
[10] R. Capote *et al.*, Nucl. Data Sheets **110**, 3107 (2009).
[11] A. R. Junghans *et al.*, Phys. Lett. B **670**, 200 (2008).
[12] A. Leprêtre, H. Beil, R. Bergère, P. Carlos, A. De Miniac, A. Veyssière, and K. Kernbach, Nucl. Phys. A **219**, 39 (1974).
[13] S. Agostinelli *et al.*, Nucl. Instr. Meth. A **506**, 250 (2003).
[14] R. Schwengner *et al.*, Nucl. Instr. Meth. A **555**, 211 (2005).
[15] L. I. Schiff, Phys. Rev. **83**, 252 (1951).
[16] R. Moreh, W. C. Sellyey, and R. Vodhanel, Phys. Rev. C **22**, 1820 (1980).
[17] F. Ajzenberg-Selove, Nucl. Phys. A **506**, 1 (1990).
[18] G. Rusev, A. P. Tonchev, R. Schwengner, C. Sun, W. Tornow, and Y. K. Wu, Phys. Rev. C **79**, 047601 (2009).
[19] R. Massarczyk, R. Schwengner, F. Donau, E. Litvinova, G. Rusev, R. Beyer, R. Hannaske, A. R. Junghans, M. Kempe, J. H. Kelley, T. Kogler, K. Kosev, E. Kwan, M. Marta, A. Matic, C. Nair, R. Raut, K. D. Schilling, G. Schramm, D. Stach, A. P. Tonchev, W. Tornow, E. Trompler, A. Wagner, and D. Yakorev, Phys. Rev. C **86**, 014319 (2012).

[20] M. Guttormsen *et al.*, Nucl. Instr. Meth. A **374**, 371 (1996).
[21] S. Raman *et al.*, At. Data Nucl. Data Tables **78**, 1 (2001).
[22] W. Andrejtscheff and R. Petkov, Phys. Lett. B **329**, 1 (1994).
[23] G. Bartholomew *et al.*, Adv. Nucl. Phys. **7**, 229 (1973).
[24] T. von Egidy and D. Bucurescu, Phys. Rev. C **80**, 054310 (2009).
[25] S. I. Al-Quraishi, S. M. Grimes, T. N. Massey, and D. A. Resler, Phys. Rev. C **67**, 015803 (2003).
[26] Y. Alhassid, S. Liu, and H. Nakada, Phys. Rev. Lett. **99**, 162504 (2007).
[27] S. Mughabghab, *Atlas of Neutron Resonance*, 5th ed. (Elsevier, Amsterdam, 2006).
[28] D. Savran *et al.*, Prog. Part. Nucl. Phys. **70**, 210 (2013).
[29] A. C. Larsen, I. E. Ruud, A. Burger, S. Goriely, M. Guttormsen, A. Gorgen, T. W. Hagen, S. Harissopulos, H. T. Nyhus, T. Renstrom, A. Schiller, S. Siem, G. M. Tveten, A. Voinov, and M. Wiedeking, Phys. Rev. C **87**, 014319 (2013).
[30] L. Szentmiklósi *et al.*, J. Radioanal. Nucl. Chem. **286**, (2010).
[31] T. Belgya *et al.*, *Proceedings for the ERINDA Workshop 2013, Geneva* (*Switzerland*) (CERN, Geneva, 2014), p. 119.
[32] D. Brink, PhD. thesis, University of Oxford, 1955 (unpublished).
[33] P. Axel, Phys. Rev. **126**, 671 (1962).
[34] C. O. Muehlhause, Phys. Rev. **79**, 277 (1950).
[35] G. Rusev, M. Jandel, M. Krticka, T. A. Bredeweg, A. Couture, T. N. Taddeucci, and J. L. Ullmann, Phys. Rev. C **87**, 054603 (2013).
[36] K. Volve *et al.*, Nucl. Instr. Meth. B **300**, 11 (2013).